Crossref
Similarity Check
Powered by iThenticate

CASO PRÁCTICO

High resolution land cover mapping and crop classification in the Loukkos watershed (Northern Morocco): An approach using SAR Sentinel-1 time series

Nizar El Mortaji*, Miriam Wahbi, Mohamed Ait Kazzi, Otmane Yazidi Alaoui, Hakim Boulaassal, Mustapha Maatouk, Mohamed Najib Zaghloul, Omar El Kharki

GéoTéCa, FSTT, Abdelmalek Essaadi University, Tetouan, Morocco.

Abstract: Remote sensing has become more and more a reliable tool for mapping land cover and monitoring cropland. Much of the work done in this field uses optical remote sensing data. In Morocco, active remote sensing data remain under-exploited despite their importance in monitoring spatial and temporal dynamics of land cover and crops even during cloudy weather. This study aims to explore the potential of C-band Sentinel-1 data in the production of a high-resolution land cover mapping and crop classification within the irrigated Loukkos watershed agricultural landscape in northern Morocco. The work was achieved by using 33 dual-polarized images in vertical-vertical (VV) and vertical-horizontal (VH) polarizations. The images were acquired in ascending orbits between April 16 and October 25, 2020, with the purpose to track the backscattering behavior of the main crops and other land cover classes in the study area. The results showed that the backscatter increased with the phenological development of the monitored crops (rice, watermelon, peanuts, and winter crops), strongly for the VH and VV bands, and slightly for the VH/VV ratio. The other classes (water, built-up, forest, fruit trees, permanent vegetation, greenhouses, and bare lands) did not show significant variation during this period. Based on the backscattering analysis and the field data, a supervised classification was carried out, using the Random Forest Classifier (RF) algorithm. Results showed that radiometric characteristics and 6 days' time resolution covered by Sentinel-1 constellation gave a high classification accuracy by dual-polarization with Radar Ratio (VH/VV) or Radar Vegetation Index and textural features (between 74.07% and 75.19%). Accordingly, this study proves that the Sentinel-1 data provide useful information and a high potential for multi-temporal analyses of crop monitoring, and reliable land cover mapping which could be a practical source of information for various purposes in order to undertake food security issues.

Key words: land cover; Sentinel-1; crop classification; time series; Loukkos watershed.

Cartografía de alta resolución de la cubierta del suelo y clasificación de los cultivos en la cuenca del Loukkos (norte de Marruecos): Un enfoque que utiliza las series temporales de SAR Sentinel-1

Resumen: La teledetección se ha convertido en una herramienta cada vez más fiable para cartografiar la cubierta vegetal y controlar las tierras de cultivo. Gran parte de los trabajos realizados en este campo utilizan datos ópticos de teledetección. Además, en Marruecos, los datos de teledetección activa siguen estando infrautilizados, a pesar de su importancia para el seguimiento de la dinámica espacial y temporal de la cubierta vegetal y de los cultivos,

* *Corresponding author: elmortajinizar@gmail.com*

incluso con tiempo nublado. Este estudio tiene como objetivo explorar el potencial de los datos de la banda C de Sentinel-1 en la producción de una cartografía de alta resolución de la cubierta del suelo y la clasificación de los cultivos dentro del paisaje agrícola de la cuenca del Loukkos de regadío en el norte de Marruecos. Este trabajo se ha realizado utilizando 33 imágenes de doble polarización vertical-vertical (VV) y vertical-horizontal (VH). Las imágenes fueron adquiridas en órbitas ascendentes entre el 16 de abril y el 25 de octubre de 2020, con el propósito de rastrear el comportamiento de retrodispersión de los principales cultivos y otras clases de cobertura del suelo en el área de estudio. Los gráficos obtenidos muestran que la retrodispersión aumenta con el desarrollo fenológico de los tres cultivos monitorizados (arroz, sandía, cacahuetes, cultivos de invierno), fuertemente para las bandas VH y VV, y ligeramente para el ratio VH/VV. Las otras clases (agua, edificado, bosque, árboles frutales, vegetación permanente, invernaderos y tierras desnudas) no muestran una variación significativa durante este periodo. A partir del análisis de retrodispersión y de los datos de campo, se llevó a cabo una clasificación supervisada, utilizando el algoritmo *Random Forest Classifier* (RF). Los resultados muestran que las características radiométricas y la resolución temporal para los 6 días cubiertos por la constelación Sentinel-1 dan una alta precisión de clasificación por polarización dual con Ratio de Radar (VH/VV) o Índice de Vegetación de Radar y características de la textura (entre 74,07% y 75,17%). En consecuencia, este estudio demuestra que los datos de Sentinel-1 proporcionan información útil y un alto potencial para los análisis multitemporales de seguimiento de los cultivos, así como una cartografía fiable de la cubierta terrestre que debería ser una fuente de información práctica para para varios propósitos a fin de acometer cuestiones de seguridad alimentaria.

Palabras clave: cubierta del suelo, Sentinel-1, clasificación de cultivos, series temporales, cuenca del Loukkos.

1. Introduction

Various earth sciences and geography domains have benefitted from the revolution of remote sensing technology and satellite imaging. For instance, land cover mapping remains one of the first products provided from satellite images analysis. These maps might provide valuable data for several research fields, such as the environment (Ullman et al., 2014), urban domain (Geymen and Baz, 2007), risk assessment (Van der Sande et al., 2003), biodiversity (Falcucci et al., 2007), and agriculture (Bargiel and Herrmann, 2011). The latter plays a crucial role in food security of a growing world population (Whelen and Siqueira, 2018), with a high impact on economic progress, by its contribution to the Gross Domestic Product (GDP) and job opportunities in agricultural activities and agricultural industry, for example in Morocco.

Several agricultural land and land cover monitoring studies are based on the optical and infrared wavelengths data ranges (Griffiths et al., 2013; Hansen et al., 2011; Yan and Roy, 2014). These images are used to calculate vegetation indexes, such as the Normalized Difference Vegetation Index (NDVI) (Jeevalakshmi et al., 2016). However, the use of these categories of satellite data is very restricted by lower availability due to

haze or clouds (Bargiel and Herrmann, 2011). With the launch of Sentinel-1 constellation providing C-band synthetic aperture radar (SAR) imagery, many scientific works revealed the importance of microwave remote sensing data for land monitoring (Balzter et al., 2015; Harfenmeister et al., 2019; Planque et al., 2021; Pulvirenti et al., 2018; Song and Wang, 2019; Suresh et al., 2016; Valcarce-Diñeiro et al., 2019).

The combination of either Sentinel-1 images data and Sentinel-2 optical data for land cover and crop mapping was applied in several countries or areas, such as Belgium (Van Tricht et al., 2018), the Chennai basin in India (Steinhausen et al., 2018), northern Malawi (Kpienbaareh et al., 2021) and the plain of Haouz which is a semi-arid area in Morocco (Moumni and Lahrouni, 2021). S1-data was also combined with other optical data such as Landsat-8 OLI (Chen et al., 2020; Kussul et al., 2016).

Other studies have proved the effectiveness of Sentinel-1 SAR data exclusively in mapping land cover and crop types, especially with the multi-temporal, multi-polarization availability, which provides accurate classes discrimination and thus improves the classification precision (Abdikan et al., 2016; Denize et al., 2019; Khalil and Saad-ul-Haque, 2018; Planque et al., 2021; Selvaraj

et al., 2019; Suresh et al., 2016; Whelen and Siqueira, 2018). This potential for crop mapping is available even on small farms (Useya and Chen, 2019), given that with the use of time series and with the RF classifier, the mapping accuracy can reach up to 96%, however using a SAR image at a single date gives unsatisfactory results. The use of radar imaging for multi-temporal classification approaches includes information on crop types and phenology to capture dynamics of the agricultural lands (Hütt and Waldhoff, 2018), and for high-resolution crop-type mapping are both widely documented in the literature (Bargiel and Herrmann, 2011; McNairn et al., 2009a). Bargiel (2017), has shown that combination of detailed information on crop phenology and multitemporal stacked Sentinel-1 images provided a suitable classification of different classes for two different growing seasons in northern Germany. Based on the temporal signatures extracted from Sentinel-1 time series, a supervised crop classification has carried out in 7 regions in the Navarre Spanish province characterized by persistent cloud cover (Arias et al., 2020). Crops like winter cereals or rice whose time signature exhibited singularities throughout the growing season achieved precise classification results. The combination of VH, VV and VH/VV time series as input features provided accurate results (Overall Accuracy OA > 70%).

The comparison of land cover classification obtained by time series Sentinel-1, RADARSAT-2, and/or ALOS-2 (Denize et al., 2019) to determine the finest SAR configuration and accurate classes identification using the RF Classifier algorithm, showed that the best SAR configuration was the S-1 time series with C-band dual polarity, although the RST-2 and ALS-2 time series also provided valuable information on the crop cover.

Sentinel-1 (S1) provides free data access which enables new possibilities to detect subtle changes in crops and fields. It can therefore be useful for agricultural crop-type mapping using multi-temporal classification approaches (Useya and Chen, 2019). Performing a successful classification requires the understanding of which growth stages are most appropriate for crop separation and identifying the SAR patterns best suited for crop classification. SAR response is very sensitive to changes in canopy structure during seed and fruit development stages that occur later in the growing

season (Mc Nairn et al., 2009b). The classification algorithm applied in our study is the RF Classifier, widely used in remote sensing for its excellent results, ability to process large datasets, and speed of execution (Pelletier et al., 2016). The use of polarization ratios, vegetation indices or textural features could improve the quality of the classification (Arias et al., 2020; Mandal et al., 2020; Zakeri et al., 2017).

The Loukkos watershed study area is one of northern Morocco's most fertile agricultural fields. However, it has not benefited from any study regarding monitoring and land cover mapping by remote sensing technology and satellite imaging. The main scientific objective of this study is to carry out a multi-temporal analysis to provide new high-resolution land cover maps and to realize an accurate classification of monitored land cover and crops belonging to the irrigated area in Laouamra village, by means of Sentinel-1 SAR data with dual-polarization (VV) and (VH) in C band, as well as to demonstrate the power of this kind of satellite data for crop discrimination. Therefore, this research focuses on the accurate monitoring of agricultural activities and the collection of agricultural database information (Brisco et al., 2017). It is the first study that analyzes and classifies the watermelon and peanut fields that are characteristic of the study area.

2. Materials and Methods

2.1. Study area and Field data

The study area is located in the rural commune of Laouamra between Ksar El Kebir and Larache cities in northwest Morocco. It belongs to the Loukkos watershed (Figure 1). The hydrogeological network of this area includes the Loukkous River, and some tributaries, and the R'mel groundwater table.

Generally, the region of Laouamra and namely the Loukkos watershed is one of the country's most productive areas for several crops, such as sugar crops, strawberries, potatoes, peanuts, vegetables, wheat, watermelon, in addition to rice that is cultivated once a year.

The studied area comprises an irrigated agricultural sandy and muddy soil nearby the Loukkos River edge. It is characterized by almost flat topography
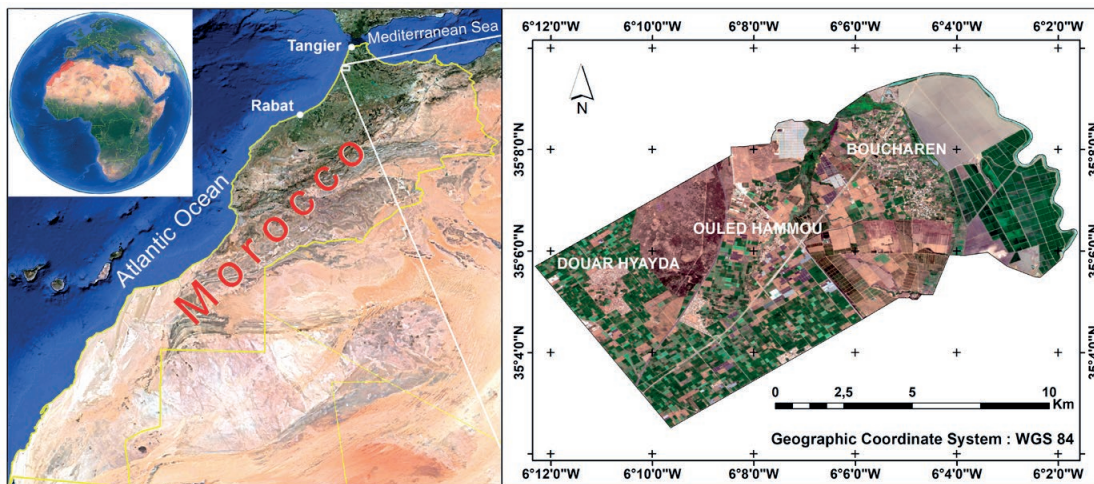
Figure 1. Geographical location of the study areas, based on Google Earth Pro images (left) and Sentinel-2 images (right) taken in August 8, 2020.

with various crop types. It is known for alternating winter crops like wheat and potatoes, and spring crops like peanuts and watermelons. Figure 2 shows the agricultural calendar of the cycles of peanuts, watermelon, rice, wheat, and potatoes to understand the backscattering behavior on the studied images.

Field visits were organized during August 2020. GPS acquisitions and photos were taken on the area characterizing the different types of land cover and crop types (Figure 3). Several areas were identified using these observations combined with photointerpretation in Google Earth Pro application and were used to calibrate and validate the supervised classification of the time series SAR Images. Figure 4 shows the distribution of calibration and validation areas represented on VH band of Sentinel-1 image sensed on April 16th, 2020. Each class received 20 areas for

calibration and 20 areas for validation, except for the uncultivated sandy soil, avocado and bare land classes which received only 10 areas as these classes have small fields. All the pixels of the training polygons are used to calibrate the classification, whereas the validation is based on the result obtained for one pixel taken randomly within each validation polygon. However, before performing the classification, the same training areas of calibration had been used to evaluate the separability between pairs of land cover classes using the means and standard deviations averages of the different polygons representing each class for all dates. In addition, the mean backscatter values of pixels were computed in the same way (Nasirzadehdizaji et al., 2021). These values would allow us to target the behavior evolution of classes using the multi-temporal backscatter analysis on the studied images.
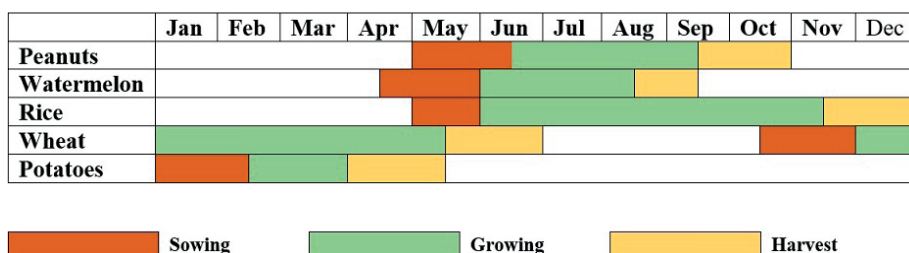

Figure 2. Peanuts, watermelon; rice, wheat, and potatoes crops calendar in the study area.

Figure 3. Land cover types photographed during field visits; (1) rice, (2) peanuts, (3) watermelon, (4) winter crops, (5) uncultivated sandy soil, (6) uncultivated muddy soil, (7) water, (8) permanent vegetation, (9) greenhouses, (10) forest, (11) citrus, (12) avocado trees, (13) bare land, (14) built-up, (15) railway.
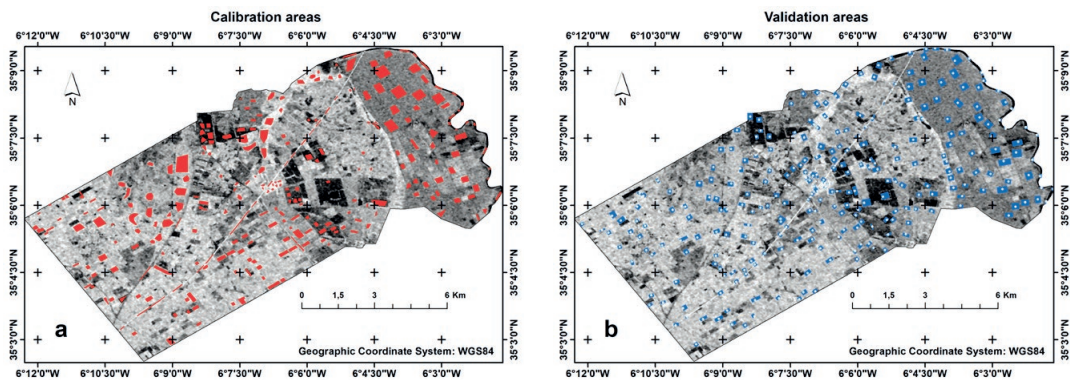
Figure 4. Supervised classification areas: (a) calibration areas with red polygons, (b) validation areas with blue polygons.

2.2. Sentinel-1 Dataset

We used in this work Sentinel-1 satellite images with exceptional high temporal resolution. The Sentinel-1 mission comprises a constellation of two twin C-band SAR satellites (Sentinel-1A and Sentinel-1B) launched in 2014 and 2016, respectively, acquiring dual polarization imagery (HH+HV or VV+VH) for earth observation regardless of the weather. The two satellite orbits are 180° apart, which allows mapping images of the entire Earth in six days (Panetti et al., 2014).

The Sentinel-1 images are taken in the Interferometric Wide (IW) swath mode and acquired in ascending orbit pass directions, in Level-1 C-band Ground Range Detected (GRD), with a 5 m×20 m spatial resolution. Incidence angles for the IW acquisition mode range from 29° to 46° and consist of focused SAR data detected and projected to the ground range using WGS84 ellipsoid model. Besides, the data used in this study (time series of 33 remotely sensed Sentinel-1 SAR, starting from April 16 to October 25, 2020) were acquired by the European Space Agency and downloaded from the data hub (https://scihub.copernicus.eu/dhus/#/home).

2.3. Methodology

To achieve the objectives of this work, we started by preparing and processing data (scenes acquisition, pre-processing, and processing stages). Later, we performed a coverage multi-temporal analysis by building backscatter profiles in VV and VH polarization for each class of crops and land cover types. Then we did a supervised land cover classification validated using confusion matrices. The main work steps are compiled and summarized in a flowchart (Figure 5).

2.3.1. Preparation steps

In order to deduce the actual intensity of the sensor's microwave signal, it is imperative to pre-process SAR images (Dimov et al., 2016). Several operations were performed using ESA's Sentinel Application Platform (SNAP). The Shuttle Radar Topography Mission (SRTM) 3sec Digital Elevation Model (DEM) was used (Figure 5).

Radar images are affected by speckle due to the coherent summation of signals scattered from ground scatterers randomly distributed in the pixels (Moumni and Lahrouni, 2021). A speckle filtering becomes necessary to reduce the granular noise (Lee et al., 1994). We applied the IDAN filter with an adaptive neighbor size of 33. After the preparation, the obtained images had a final spatial resolution of 10 m×10 m pixel spacing.

With the aim to improve the dual-pol images classification results by providing a better discrimination between classes, we used the Radar Vegetation Index (RVI) through calculation from the processed images. The same was done with the textural features analysis (Szantoi et al., 2013). Also the VH/VV polarization ratio was found to be useful in crops monitoring (Arias et al., 2020).

RVI is a parameter sensitive to the biomass level; it increases with crop growth and decreases with the reduction of vegetation water content (Yunjin and van Zyl, 2009). RVI was designed to monitor the
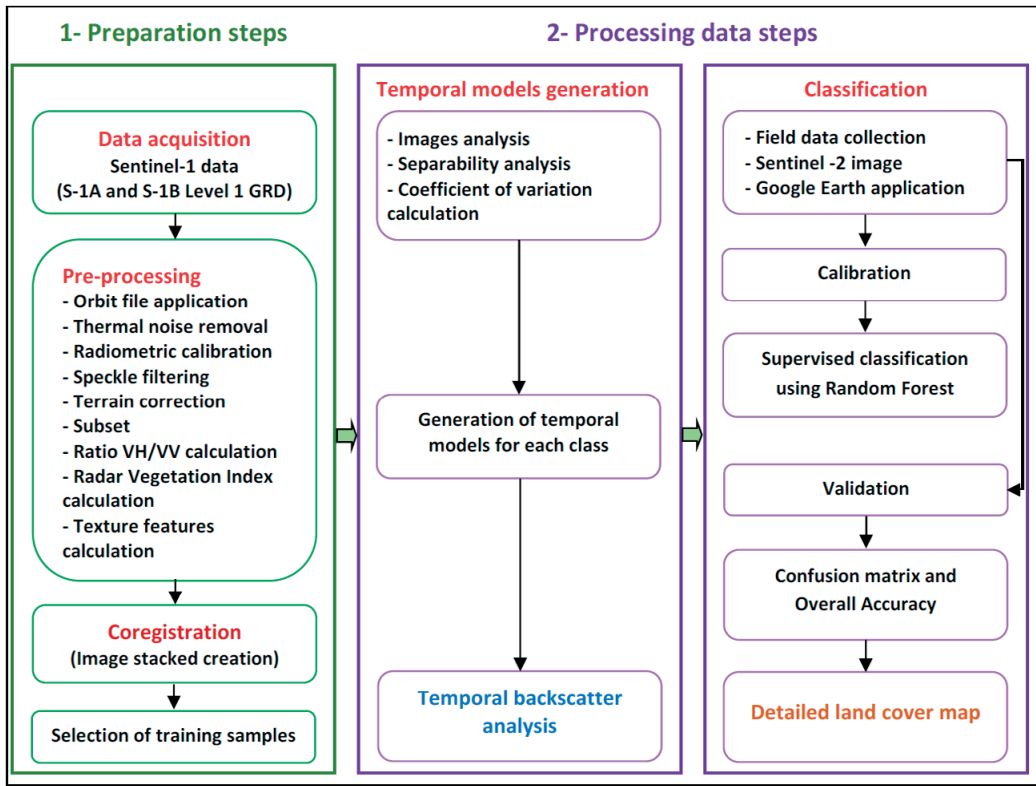
Figure 5. Flowchart of the methodology.

vegetation growth in time series data analysis as an alternative to Normalized Difference Vegetation Index (NDVI) used in optical image processing studies (Kumar et al., 2013). Both RVI and NDVI are obtained from the combination of different satellite bands. The original RVI was developed for quad polarization radar imagery (Yunjin and van Zyl, 2009). To adapt the use of RVI for dual Pol SAR images such as Sentinel-1 images, Nasirzadehdizaji et al. (2019) suggested the Equation 1.

$$RVI = \frac{4\sigma^0\,VH}{\sigma^0\,VV + \sigma^0\,VH'} \qquad (1)$$

Texture analysis is an inherent spatial feature of an image, as SAR backscatter is sensitive to the type, orientation, homogeneity and spatial relationship of ground objects (Zeng et al., 2010). Among four groups of texture analysis methods, the statistical methods based on the gray-level co-occurrence matrix (GLCM) seem to be the most used. They use the characteristic of spatial correlation of gray values to describe the texture (Zeng et al., 2010).

The GLCM indicates the probability that values of each pair of pixels co-occur in each direction and at a certain lag distance in the image (Haralick et al., 1973). In this study, 3 texture features were calculated, the mean, the variance, and the correlation.

2.3.2. Processing steps:

We analyzed images with different polarizations and polarimetric (RGB) composites for a giving date, or different dates to discriminate various land cover classes. A separability analysis was also identified as a good indicator of class discrimination (Vanniel et al., 2005). Features are well separated if the distance between the class mean values is large compared to the standard deviations (Jiancheng et al., 1994). The separability (S) between classes i and j is defined by Equation 2.

$$S_{i,j} = \frac{|\mu_i - \mu_j|}{s_i + s_j} \qquad (2)$$

Where μ and s are mean values and standard deviations of the features. Separation values $S_{i,j}$ below 0.8 are not large enough to be useful in distinguishing class i from class j. For values of $S_{i,j}$ between 0.8 and 1.5, the quality of the separation between classes i and j is average. Values of $S_{i,j}$ above 2.0 provide almost complete separation of class pairs (Baghdadi et al., 2001). The separability has been calculated for all dates. Furthermore, three distant dates were analyzed in detail (April 16, 2020, July 15, 2020, October 13, 2020).

The coefficient of variability (CV) was also used (Equation 3). It is a unitless statistical measurement of variation with values from 0 to 1, defined in probability theory and statistics by the ratio of the standard deviation of the signal (s) by the mean value (μ) (Whelen and Siqueira, 2018).

$$CV = \frac{s_i(\sigma)}{\mu(\sigma)} \qquad (3)$$

CV was computed from time series with VH or VV bands in SNAP software for pixels occupying the same location on the multi dates images. It allowed us to distinguish the classes' changes throughout the different phases.

One of the main processing steps focuses on generating temporal models from multi-temporal intensities using SNAP software to characterize the changes in classe structure during the study period and, therefore, separate the different classes. The mean backscatter values were calculated in the VV and VH polarizations, and the VH/VV polarization ratio.

The supervised classification approach we used is a "pixel-based" approach using the RF algorithm which consists of a combination of tree classifiers where each classifier is generated using a random vector sampled independently from the input vector, and each tree casts a unit vote for the most popular class to classify an input vector (See additional details in Breiman, 1999). For each case, we selected 5000 training samples, and 200 trees. For the SAR time series, the temporal signatures allow the determination of each class, and this permits identifying whether an unknown field belongs to one class or another. 15 classes were chosen:1) Rice, 2) Peanuts, 3) Watermelon, 4) Winter crops, 5) Uncultivated sandy land, 6) Uncultivated muddy land, 7) Water, 8) Permanent vegetation, 9) Green houses, 10) Forest, 11) Citrus, 12) Avocado trees, 13) Bare land, 14) Built-up, and 15) Railway.

According to seven scenarios, we have chosen to map the land cover from Dual Pol SAR Sentinel-1 image (Table 1). To determine the best performing scenario quantitatively, we grouped the obtained results into confusion matrices tables. Finally, we used these tables to calculate several accuracy parameters such as, User's Accuracy (UA), Producer's Accuracy (PA), Overall accuracy (OA), and Kappa coefficient (K).

3. Results and Discussion

3.1. Separability between classes

According to the mean separability values (Figure 6), the VH and VV polarizations gave a higher separability between classes than VH/VV polarization ratio. Generally, separability values obtained by VH are better than those obtained by VV, except in a few cases where VV shows the best values, for instance, separability between water and greenhouses, or between water and watermelon or rice.

Table 1. The different scenarios proposed for the supervised classification.

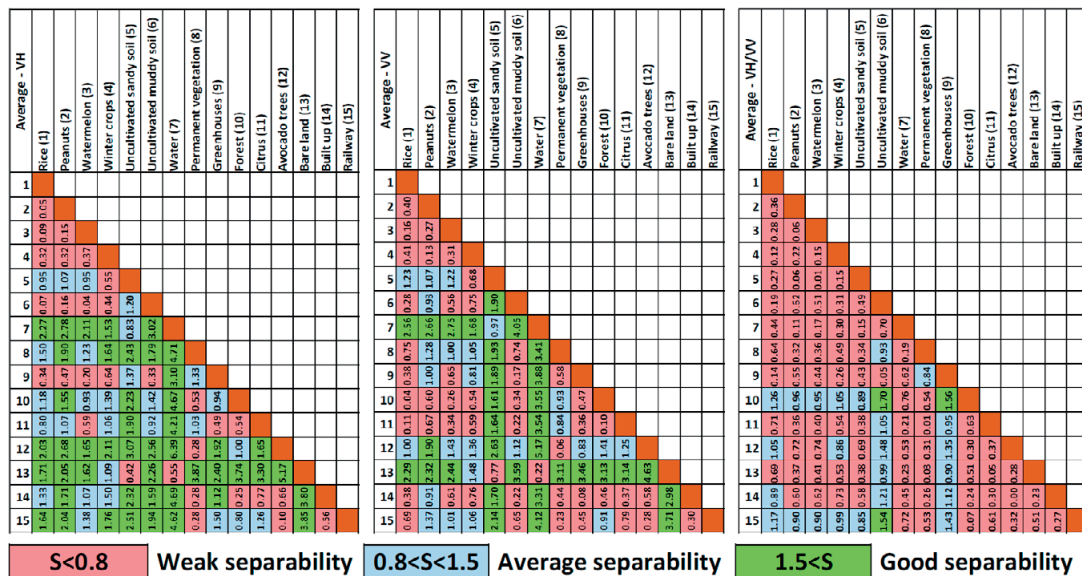| Stacked Image	Bands
Single image (August 08, 2020)	VV, VH polarization
Time series	VV polarization.
	VH polarization.
	VV + VH polarizations.
	VV + VH polarizations + the ratio VH/VV;
	VV + VH polarizations + Radar Vegetation Index (RVI);
	VV + VH polarizations + Texture

Figure 6. Mean separability calculation between pairs of classes obtained for time series backscatter in VV, VH and VH/VV polarizations, during the whole study period.

Legend: **S<0.8** Weak separability | **0.8<S<1.5** Average separability | **1.5<S** Good separability

According to the separability values obtained by the VH polarization, the rice, peanuts, watermelon, and winter crops show low values when compared to each other and uncultivated muddy soil and greenhouses classes. In contrast, these values are well compared with other classes. Uncultivated muddy soil class has low separability with the greenhouses class, which gives a low separability with the citrus class. Uncultivated sandy soil class exhibits a medium to good separability with almost classes, except winter crops and bare lands, showing low separability values. Similarly for water class, which has good separability values with most of classes, except bare land class which is hardly separated from uncultivated sandy soil. The permanent vegetation has low separability with forest, avocado trees, and medium separability with citrus trees. Forest has low separability with citrus trees and built-up and medium to good separability with other classes. The built-up and railway classes are hardly separated from each other and other classes like permanent vegetation and avocado trees.

The separability at three distant dates is shown in Figure S1 in supplementary material section. Separability between rice and other crops becomes better in October compared to April and July for VH and VV. Separability between the fields of peanuts and watermelon was average in April and decreased in July and October. However, separability between peanuts and winter crops was average on the three dates. Separability between watermelon and other classes is better in July. Separability values are optimal in July between the three classes (uncultivated sandy soil, uncultivated muddy soil, and greenhouses), and the other classes. Water shows a better separability with other classes in April by the VV polarization. This polarization also provides a good separability to bare land in July. Permanent vegetation, forest, citrus, and avocado trees classes have almost the same separability values for the three dates. The separability between built up and the other classes improves in October, except with rice class. The same statement is true for the railway.

To sum up, separability is therefore good for varied classes, such as, crops that change in structure and length during phenological development. In this case, VH bands give a better result compared to VV bands. Less important for relatively smooth surfaces, VV bands allow better discrimination between classes, and low for tree classes and rough surfaces. The results are almost the same for VH and VV. In all cases, VH/VV present the least satisfactory results.

3.2. Coefficient of variation calculation

The results of CV (Figure 7) allow identifying areas with high CV (rice, peanuts, watermelon, winter crops), and areas with low CV (trees, water, bare land, uncultivated soil, built-up, railway). In general, the time series images with VH polarization give higher CV values compared to the time series with VV polarization for peanuts, watermelons, and winter crops, while the time series images with VV polarization show relatively high CV values compared to VH polarization for rice fields.

3.3. Temporal backscatter analysis

3.3.1. Data analysis

The mean and the standard deviation values of the backscatter are shown in Figure 8. Both VV and VH show a similar backscatter evolution trend, only intensity differs. Each field shows a unique pattern that depends on land cover, phenology, moisture content, and soil type.

The values of the backscatter signal for both polarizations in rice fields show a clear change. Before June, backscatter values were around -20 dB for VH, between -10 dB and -12 dB for VV and around -10 dB for VH/VV. During June, there was a remarkable decrease in the backscatter reaching ~-28 dB in VH and ~-20 dB in VV, while the VH/VV values remain high (around -10 dB). The backscatter increases again from the beginning of July until the beginning of August to reach maximum values. After this date, the

backscatter values remain almost stable for VV (~-10 dB), while it continues to increase slightly for VH and VH/VV (-19 dB to -17 dB, -10 dB to -7 dB respectively).

The evolution of backscatter in peanut fields is characterized by three distinct phases: the backscattered signal increases progressively from mid-May to mid-July, from -25 dB to -14 dB for VH polarization, and from -18 dB to -9 dB for VV polarization, and from -10 dB to -7 dB for VH/VV. After a stability period until the end of September, the backscatter signal of VH and VV polarizations decreases during the harvest period. The values of VH/VV polarization ratio show a slight variation during the increased and decreased backscattering phases.

The backscatter of the watermelon class starts with almost stable and low values for the three polarizations. From mid-June to mid-July the VH backscatter has increased rapidly and strongly (from -27 dB to -15 dB) relative to the VV polarization (from about -13 dB to -8 dB). The VH/VV backscatter changes slightly. Until the end of August, the backscattering values remain at their maximum and decrease to reach low values during September.

The signal of both polarizations for winter crops represented by wheat was strong till beginning of July (~-19 dB for VH, ~-12 dB for VV), and decreased after this date, to stable and lower values (~-25 dB for VH, ~-14 dB for VV). Whereas, the VH/VV polarization ratio remains almost stable with few fluctuations and a slight decreasing trend from July to August.
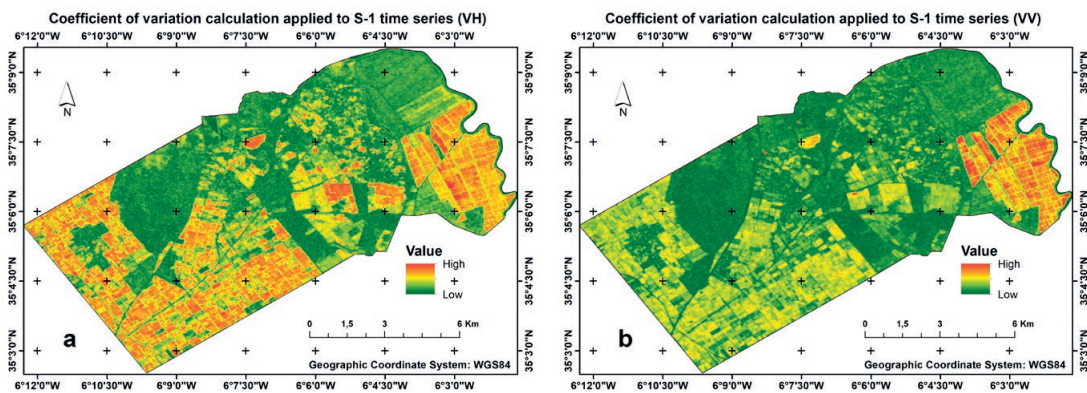
Figure 7. Coefficient of variation (CV) for VH polarization (a) and VV polarization (b).
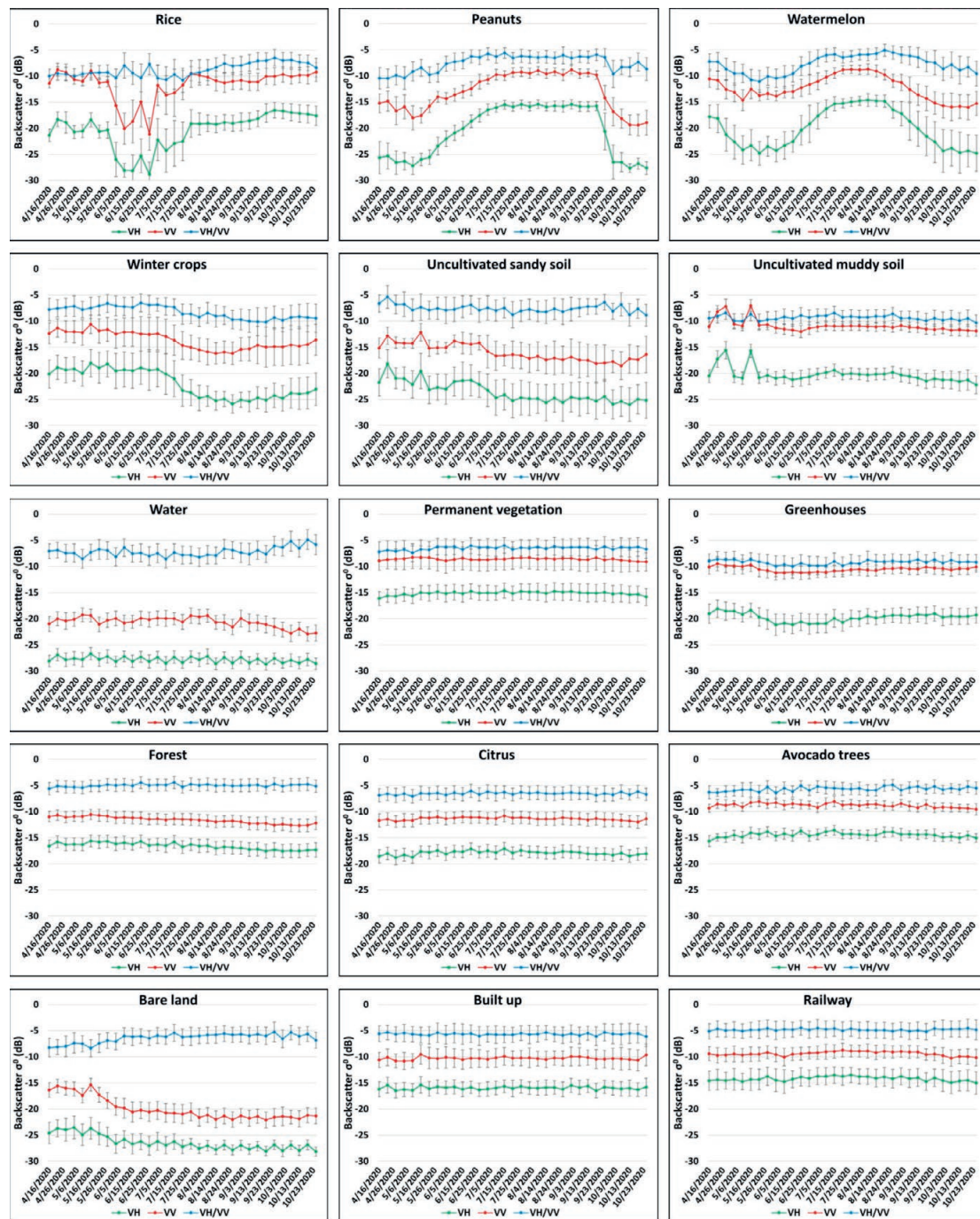
Figure 8. Temporal behavior of the backscattering coefficients (σ^0 dB) of the different land cover classes, in VH, VV polarizations, and VH/VV ratio calculated. standard deviations at each date are represented by error bars.

The uncultivated sandy soil backscattering behavior shows values irregularity. The backscatter progressively decreases slightly for all three polarizations (from ~-21 dB to ~-25 dB for VH, from ~-14 dB to ~-17 dB for VV, and from ~-03 dB to ~-08 dB for VH/VV) from the beginning of the study period until mid-July, after which the values stabilize. The uncultivated land

on muddy soil, around rice crops, does not exhibit a large variation in backscatter signal for both polarizations (~-20 dB for VH, ~-11 dB for VV and ~-9 dB for VH/VV), except during the period before the end of May, when the backscatter fluctuates between – 19 dB and -14 dB for VH, and between – 11 dB and – 7 dB for VV.

Water shows a very low backscatter signal in VH and VV polarizations (~-20 dB for VV and ~-25 dB for VH) due to the calm surface appearance of scattering. VH/VV polarization ratio takes values between -8 dB and -5 dB. Bare land also has low backscatter values which remain almost stable throughout the year, given the lack of sufficiently developed vegetation and the unchanging soil texture. The highest values have been recorded before the dry season when the vegetation linked to rainfall persists.

Fruit trees (citrus and avocado), forest trees and permanent vegetation show strong and almost stable backscattering with slight variation over the period of the study. Generally, the backscatter values are around -14 dB to -18 dB for VH, -8 dB to –11 dB for VV, and ~-6 dB for VH/VV. Other classes have almost the same values as the tree classes, these classes are built-up and railway: They show strong and stable backscatter signals. Greenhouse crop fields exhibit strong backscattering in VV and VH/VV polarizations (~-10 dB) and medium values on backscatter in VH polarization (~-20 dB) with slight variation.

We also observe that the standard deviation values of each date are generally low and almost stable in VV, VH, and VH/VV polarizations (between ~1 dB and ~2 dB), for classes with stable mean backscatter profiles (water, permanent vegetation, greenhouses, uncultivated muddy soil, forest, citrus, avocado trees, bare land, built up, and railway). However, the variability in backscatter is relatively large, especially at the beginning and the end of the crops' life cycle (peanuts, watermelon, and rice), which show high values of standard deviation (between ~2 dB and ~4 dB), for all three polarizations, unlike the backscatter stability phase where the standard deviation is ~1 dB. For the uncultivated sandy soil and winter crops classes, the standard deviation values are between ~2 dB and ~3 dB during almost all dates.

3.3.2. Data interpretation

The backscatter variation during the vegetation period can be explained by the varying contribution of soil and vegetation as well as by structural changes of the plants and their water content (Harfenmeister et al., 2019). As growth stages vary according to the crop type, biomass accumulation changes the structure of the crop canopy which helps to differentiate various crop types (McNairn and Shang, 2016). The main obtained results for type-crops during the April-October period are congruent with those reported by Arias et al. (2020), where backscattering was linked to different phases (sowing, growth, and harvest phases). The growth phase can be divided into several phenological stages of plant development according to the Biologische Bundesanstalt, Bundessortenamt, and CHemische (BBCH) scale (Munger et al., 1998).

During May, rice fields were ploughed and then submerged and sown at the beginning of June (Clauss et al., 2018; Mandal et al., 2018). This explains the variations of the backscatter, because the backscattering values in May are linked to the surface roughness of the plowed muddy soil which scatters the waves in the VV and VH polarizations significantly. These values decrease considerably when the fields are flooded in early June because of specular reflection from standing water, while the VH/VV values remain high (Arias et al., 2020; Ndikumana et al., 2018; Torbick et al., 2017). With water infiltration and plant growth, the backscatter for both VH and VV polarizations increases steadily from early July until mid-August, as the volume of the plant increased and reaches the maximum vegetative stage. This is also related to the dielectric constant of the target, and it increases when the water content of the vegetation increases (Nelson et al., 2014). After mid-August, the backscatter depends on the rice canopy which becomes denser during the tillering phase. Normally, the rice of the Loukkos watershed is harvested from the end of November until December. For this reason, the rice backscattering profiles show the absence of the harvest phase.

In addition, all three phases are very well recorded for peanuts. Around mid-May, a large part of sandy soil fields is plowed and sown with peanut seeds, which explains the low backscatter values

for the three polarizations during this period compared to backscatter values in plowed muddy soil, as these are more rigorous than sandy soils. The backscatter is thus linked during this phase to the soil structure essentially. But, with the gradual growth of seedlings in the early vegetative stage, biomass increases and so does plant size with regular irrigation, which influences the interaction with the radar waves, and thus the time series profiles show a progressive increase of the backscatter for VH, VV and VH/VV, with a high intensity of VH and VV compared to VH/VV. The backscatter reflects the influence of seedlings size, increasing biomass, water content of the seedlings, and soil moisture. Backscatter values recorded in mid-August show that peanut plants have reached maturity with the maximum size and leaf area. Directly after this date, there is a slight decrease in the intensity of backscatter related to a decrease in biomass and water content of the plants. After harvest, the backscatter values decline for VH and VV and return to the values of the sowing phase, because of direct interaction with the soil.

Watermelon fields also show all three phases, with remarkable differences in the duration of each phase. During the growth phase, we can differentiate two stages (vegetative and reproductive). Tilling of watermelon fields on sandy soil does not begin until late May. With intense irrigation, watermelon seedlings grow rapidly by early June, and leaf mass becomes significant. This explains the significant increase in backscatter intensity for VH relative to the slight increase of VV and VH/VV. With the appearance and growth of watermelon, the interaction between waves and objects becomes important, and a peak in backscatter is recorded for the VV polarization around mid-August. When mature fruits are collected, the plants remain on site for a few days before being pulled out, which explains the rapid decrease in backscatter of all three polarizations around early September. A few days later, as the irrigated region is known for alternating the two crops each year for the same plot, the land is reworked again to prepare for a new winter crop. It is recorded on the backscatter profiles by a further increase of the backscatter values.

For winter crops -represented by wheat- the last two phases have been recorded on the profiles: i) the growth phase which corresponds to high backscatter signal values, and ii) the harvest and post-harvest phase marked by a decrease in the backscatter signal.

The monitoring of the backscattering behavior in the cultivated fields shows that the VH backscatter is generally more sensitive to volume scattering from the vegetation, and to the soil in the early phenological stages. Thus, the VH backscatter is mainly affected by the double stem-ground scattering (Brown et al., 2003). In addition, the water content and soil moisture have an influence. On the other side, the VH/VV polarization ratio shows slight variations, especially in the early phenological stages, but has greater stability compared to the simple VH and VV polarizations, since factors influencing the backscatter characteristics, such as humidity or radiometric instability of the sensor, are compensated by the ratio (Veloso et al., 2017).

The strong backscattering signal of fruit trees and forest can be explained by the unchanging structure of almost all trees beside the roughly dense foliation related to the tree type. Besides, the dense vegetation near water points and rivers throughout the year allows strong and stable backscattering values.

By comparing the backscatter values of the uncultivated sandy soil class prior to June, with the other classes values, these values correspond to other winter crops, most probably potatoes because the pattern of the backscatter profiles towards the end of the wheat cycle is different. This may explain why those plots have been reworked during summer (period of field visits), to get rest and prepare for a new crop after August.

The uncultivated muddy soil displays little variation in backscatter during the month of May, due to the plowed yet unsown and unirrigated lands with rough surface characterized by a strong backscatter signal. With time the soil becomes less rugose, allowing for almost stable backscatter during the rest of the study period.

The high variability in backscatter from rice fields at the beginning of the season can be explained by the fact that fields at this stage have a variety of states, from bare fields, flooded or not, to rice plants at different stages of growth (Phan et al., 2021). While this variability for the peanuts and

watermelon classes is mainly explained by the fact that planting and harvesting calendar may be different, as the fields are not cultivated and harvested at the same time. In addition, winter crops fields may have different crop types and management.

The analysis of the backscatter profiles and standard deviation values showed that our knowledge of the phenological phases of the studied crops can be useful in interpreting the backscatter variations extracted from Sentinel-1 time series. Conversely, from these time series we can understand the temporal dynamics of crops. Thus, crops with distinct backscatter profiles would be discriminable in supervised classification. However, classes with similar backscatter profiles with no variation over time would cause difficulties in discriminating from each other.

3.4. Land cover and crop mapping

3.4.1. Accuracy assessment

Land cover and crop mapping were obtained by supervised classification of different images according to the aforementioned scenarios (Figure S2 in supplementary materials section). The approach used in this work made it possible to obtain maps of land cover and crops, with varying accuracy parameters, particularly for (OA) and (K) parameters (Figure 9).

The single-date image pattern provided the lowest values of OA (31.48%) and K (0.26) compared to other scenarios. With the use of time series, OA improves significantly. The comparison between the time series with the VH bands and those composed VV bands shows that VH presents a more satisfactory OA (70%) and K (0.68) than VV (OA=66.67 and K= 0.64). With a multi-temporal image with two polarizations VH and VV, the values of OA reaches the value 71.11% and K the value 0.69. The inclusion of other bands (VH/ VV polarization ratio, RVI, Texture) to the time series with two polarizations allowed us to obtain an improvement of 3% to 4% for OA and 0.3 to 0.4 for K. The best scenario with a time series image is composed of the bands VV, VH and Texture, according to the values of OA (75.19%) and K (0.73).

With reference to the values of F1-score, UA, and PA for each class according to the proposed seven scenarios (Table 1), we find that the single date image presents the least satisfactory results with low F1 values, and which do not exceed 0.5 for all classes. Thus, the values of PA and UA are below 50% for all classes, except the water class which
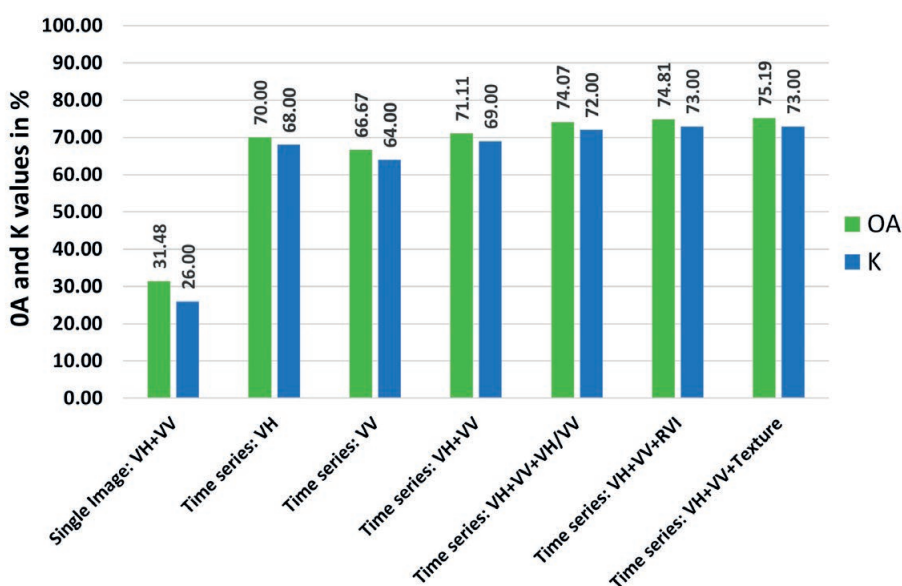

Figure 9. Evolution of Overall Accuracy (OA) and Kappa Coefficient (K), according to the different proposed scenarios.

Table 2. User's Accuracy, Producer's Accuracy and F1-Score of the different classes, Overall Accuracy and Kappa Coefficient, obtained with a supervised classification using Random Forest Classifier; (PA) Producer's Accuracy, (UA) User's Accuracy, (OA) Overall Accuracy, (K) Coefficient of Kappa.

	Single Image VH, VV			Time series VH			Time series VV			Time series VH, VV			Time series VH, VV, VH/VV			Time series VH, VV, RVI			Time series VH, VV, Texture		
	UA (%)	PA (%)	F1-Score	UA (%)	PA (%)	F1-Score	UA (%)	PA (%)	F1-Score	UA (%)	PA (%)	F1-Score	UA (%)	PA (%)	F1-Score	UA (%)	PA (%)	F1-Score	UA (%)	PA (%)	F1-Score
Rice	18.52	25	0.21	100	100	1	100	95	0.97	100	85	0.92	100	90	0.95	100	95	0.97	100	100	1
Peanuts	36.84	35	0.36	100	85	0.92	100	95	0.97	94.74	90	0.92	94.44	85	0.89	100	85.71	0.92	90	90	0.90
Watermelon	23.08	25	0.24	86.96	100	0.93	95.24	100	0.98	90.48	95	0.93	86.36	95	0.90	86.36	100	0.93	81.82	90	0.86
Winter crops	40	62.5	0.49	73.08	95	0.83	69.57	80	0.74	70.37	95	0.81	71.43	100	0.83	74.07	100	0.85	60.61	100	0.75
Uncultivated sandy soil	27.27	30	0.29	100	20	0.33	50	20	0.29	100	40	0.57	71.43	50	0.59	75	60	0.67	100	20	0.33
Uncultivated muddy soil	42.86	30	0.35	100	90	0.95	100	90	0.95	100	90	0.95	100	90	0.95	100	90	0.95	100	85	0.92
Water	64.71	55	0.59	93.33	70	0.80	100	95	0.97	100	95	0.97	100	100	1	100	100	1	83.33	100	0.91
Permanent vegetation	42.86	45	0.44	60	15	0.24	50	10	0.17	33.33	20	0.25	100	10	0.18	80	20	0.32	100	25	0.40
Greenhouses	20	20	0.20	70.59	60	0.65	40	40	0.40	69.23	45	0.55	75	45	0.56	83.33	50	0.63	73.33	55	0.63
Forest	28.57	40	0.33	72.73	40	0.52	57.89	55	0.56	75	45	0.56	73.33	55	0.63	71.43	50	0.59	83.33	50	0.63
Citrus	14.29	10	0.12	60.87	70	0.65	41.94	65	0.51	50	80	0.62	54.84	85	0.67	48.48	80	0.60	60.87	70	0.65
Avocado trees	0	0	0	71.43	50	0.59	50	80	0.62	50	70	0.58	50	80	0.62	61.54	80	0.70	45.00	90	0.60
Bare land	41.67	50	0.45	47.37	90	0.62	90.91	100	0.95	76.92	100	0.87	100	100	1.00	100	100	1	100	50	0.67
Built up	14.29	10	0.12	35.14	65	0.46	11.11	5	0.07	33.33	30	0.32	45	45	0.45	42.86	30	0.35	50	70	0.58
Railway	43.75	35	0.39	50	75	0.60	37.84	70	0.49	54.84	85	0.67	51.52	85	0.64	48.65	90	0.63	83.33	100	0.91
OA	31.48%			70.00%			66.67%			71.11%			74.07%			74.81%			75.19%		
K	0.26			0.68			0.64			0.69			0.72			0.73			0.73		

gives PA=55% and UA=64.11%. For scenarios with multi-temporal images, the different classes can be organized under four groups (Table 2):

i) A first group contains classes with an F1-score greater than 0.75 for all scenarios (rice, peanuts, watermelon, winter crops, uncultivated muddy soil, and water).

The rice class presents the most satisfactory F1-score PA and UA values (0.92≤F1-score≤1), with UA=100 for all scenarios and PA=100% for VH and VH+VV+Texture, PA=95% for VV and VH+VV+RVI, whereas for VH+VV and VH+VV+VH/VV the PA value is 85%.

The peanuts class presents F1-score between 0.89 obtained for VH+VV+VH/VV with UA=94.44% and PA=85%, and 0.97 obtained for VV with UA=100% and PA=95%. The VH, VH+VV, and VH+VV+RVI scenarios provided an F1-Score=0.92 and relatively balanced AU and PA, while F1-score=0.90 with the same UA and PA for VH+VV+Texture.

The watermelon class shows F1-score values ranging from 0.86 for VH+VV+Texture (UA=81.82% and PA=90%) to 0.98 for the VV scenario. The VH, VH+VV, and VH+VV+RVI scenarios have an F1-score=0.93, while F1-score for VH+VV+VH/VV is equal to 0.9.

The winter crops results are the least satisfactory compared to the three previous crop classes, since the F1-score values are between ~0.75 for VV (UA=69.57% and PA=80%) and VH+VV+Texture (UA=60.61% and PA=100%), and 0.85 for VH+VV+RVI (AU=74.07% and PA=100%). VH and VH+VV+VH/VV have a value of F1-score 0.83 with PA greater than UA, and the time series VH+VV presents UA=70.37% and PA=95%, which gives a value F1-score=0.81.

Uncultivated muddy soil class presents a value of F1-score=0.95 (UA=100% and PA=90%) except for the last scenario VH+VV+Texture, where the F1-score decreases to 0.92 with the decrease of PA to 85%. The water class values are in the range F1-score=0.80 (UA=93.33% - PA=70%) for the VH scenario, and F1-score=1 for VH+VV+VH/VV and VH+VV +RVI. The VV and VH+VV scenarios have a value of F1-score 0.97 (UA=100% and PA=95%). VH+VV+Texture gave an F1-score value of 0.91, with UA=83.33% and PA=100%.

ii) A Second group contains the classes with an average F1-score (0.5≤F1-score≤0.75). It comprises the forest and citrus classes.

The forest class exhibits F1-score values between 0.52 obtained for VH and 0.63 obtained from the time-based images VH+VV+VH/VV and VH+VV+Texture, thus the values of UA are

higher than that of PA for all scenarios. The F1-score values of the citrus class are in the range of 0.51 for VV (UA=41.94% – PA=65%) and reach 0.67 for VH+VV+VH/VV, with UA=54.84% and PA=85%. The avocado trees class has F1-score values between 0.59 for the VH scenario (UA=71.43% and PA=50%) and 0.70 for the VH+VV+RVI scenario (UA=61.54% – PA=80%). We can add the greenhouses class to this group, which gives average values of F1-score for all scenarios (0.55≤F1-score≤0.65) except the VV scenario where a value of F1-score 0.40 is obtained.

iii) A third group includes classes with F1-score values below 0.50 for almost all scenarios. This group consists of two classes: Permanent vegetation and built-up. The first class has F1 score values between 0.17 for VV (UA=50% – PA=10%) and 0.40 for VH+VV+Texture (UA=100% - PA=25%). The second class has F1-score values lower than 0.5 except for VH+VV+Texture which gave F1-score=0.58. The classification according to the time series scenario at VV gave the lowest F1-score value with very low values of UA (11.11%) and PA (5%), the other values of F1-score vary from 0.32 to 0.46 according to each model.

iv) A fourth group contains three classes with widely variable F1-scores from one scenario to another. The bare land class results show that the VH and VH+VV+Texture scenarios provide average F1-score values (0.62 and 0.67 respectively). The other scenarios yielded better values ranging from F1-score=0.87 (UA= 76.92% – PA= 100%) for VH+VV to 1 for VH+VV+VH/VV and VH+VV+RVI, going through F1-score=0.95 of the VV scenario (UA=90.91% - PA=100%).

The F1-score values of the uncultivated sandy soil class move between low values below 0.50 according to the VH, VV and VH+VV+Texture scenarios (0.33, 0.29 and 0.33 respectively), and average values between 0.50 and 0.75 for VH+VV, VH+VV+RVI and VH+VV+Texture (0.57, 0.59, 0.67 respectively), UA and PA values are unbalanced and vary from scenario to scenario.

The three F1-score intervals are covered by the railway classification. The VV polarization provided the lowest value among the different scenarios (0.49) with UA=37.84% and PA=70%, while the VH+VV+Texture scenario gave satisfactory values (F1-score=0.91, UA= 83.33% and PA=100%) allowing better discrimination of this class according to this model. The other scenarios provided intermediate values.

Based on this analysis, it can therefore be considered that the most satisfactory scenarios to improve discrimination between the different classes of land cover in the study area are limited to images of the time series VH+VV+RVI and VH+VV+Texture due to their high values of OA and K parameters (Table 2), as well as their improvement of the UA and PA parameters for several classes. Both scenarios have the same value of K (0.73), with a slight improvement in OA for VH+VV+Texture, compared to VH+VV+RVI (75.19% and 74.81% respectively). Despite this comparison, the VH+VV+RVI scenario presents relatively better F1-score, UA, and PA values than VH+VV+texture for some classes, especially the crop classes. However, combining these statistical results with the maps obtained by supervised classification, allows us to conclude that the VH+VV+Texture scenario remains more relevant. To this end, it can be considered that this scenario is the most favorable to produce a high-resolution map of land cover and crop types. Table 3 exhibits the detailed confusion matrix of the supervised classification obtained from this model.

For the VH+VV+Texture time series image scenario, rice, winter crops, water, and railway classes have an excellent accuracy up to 100%. Other classes show high accuracy values such as peanuts, watermelon, avocado trees (90%), and uncultivated muddy soil (85%). The latter values result from low confusion between the classes, like the confusion between peanuts and watermelon, where the incorrectly classified peanut fields were assigned mainly to the watermelon class, and vice versa. Avocado trees with citrus, and uncultivated muddy soil with watermelon (Omission Error=10%) and winter crops (Omission Error=5%).

Otherwise, classes show medium accuracy value; the citrus class has a value of 70 % and presents confusion with built-up and greenhouses classes with values of omission error of 25% and 5% respectively. The same accuracy value was obtained by built-up class, which gives 15 % as confusion with railway, 10% with citrus, and

Table 3. Confusion matrix of the supervised classification using RF Classifier of a stack time series image with bands in VV, VH polarizations and Textural features.

	Ground Truth (%)														
	Rice	Peanuts	Watermelon	Winter crops	Uncultivated sandy soil	Uncultivated muddy soil	Water	Permanent vegetation	Greenhouses	Forest	Citrus	Avocado trees	Bare land	Built-up	Railway
Rice	100	0	0	0	0	0	0	0	0	0	0	0	0	0	0
Peanuts	0	90	10	0	0	0	0	0	0	0	0	0	0	0	0
Watermelon	0	10	90	0	0	10	0	0	0	0	0	0	0	0	0
Winter crops	0	0	0	100	70	5	0	0	20	0	0	0	10	0	0
Uncultivated sandy soil	0	0	0	0	20	0	0	0	0	0	0	0	0	0	0
Uncultivated muddy soil	0	0	0	0	0	85	0	0	0	0	0	0	0	0	0
Water	0	0	0	0	0	0	100	0	0	0	0	0	40	0	0
Permanent vegetation	0	0	0	0	0	0	0	25	0	0	0	0	0	0	0
Greenhouses	0	0	0	0	10	0	0	0	55	10	5	0	0	0	0
Forest	0	0	0	0	0	0	0	5	0	50	0	0	0	5	0
Citrus	0	0	0	0	0	0	0	5	15	10	70	10	0	10	0
Avocado trees	0	0	0	0	0	0	0	45	0	10	0	90	0	0	0
Bare land	0	0	0	0	0	0	0	0	0	0	0	0	50	0	0
Built-up	0	0	0	0	0	0	0	15	10	20	25	0	0	70	0
Railway	0	0	0	0	0	0	0	5	0	0	0	0	0	15	100
Omission Error (%)	0	10	10	0	80	15	0	75	45	50	30	10	50	30	0

5% with forest. Greenhouses class on the other side has an accuracy value of 55% and presents confusion with winter crops (20%), citrus (15%), and built-up (10%).

On the other hand, four classes (permanent vegetation, uncultivated sandy soil, forest, and bare land) show low accuracy values between 20% and 50%. The two classes' forest and bare land have the value of 50% as accuracy, while the first one has confusion with built-up (20%), avocado trees, citrus, and greenhouses (10%) each one. The second has confusion with water (40%), and winter crops (10%).

The lowest accuracy values were recorded by permanent vegetation (25%) and uncultivated sandy soil (20%) due to large confusions with other classes. A significant number of pixels that should be assigned to permanent vegetation class were incorrectly classified as avocado trees (OE=45%) or built-up (OE=15%) or forest, citrus, and railway (5% as OE each one). Uncultivated sandy

soil is the least correctly classified class, with confusion that reaches 80% spread over winter crops (70%) and greenhouses class (5%). These classes with lower accuracy values contributed to the decrease in the overall accuracy and the Kappa coefficient.

3.4.2. Data interpretation

The supervised classification carried out in this work is based on the temporal signature of the different classes studied using the RF as an algorithm. The results obtained vary significantly from one scenario to another and within the classes, where the crops presenting unique and specific features in their temporal signatures are the best classified. In general terms, the findings demonstrate that the multi-temporal classification based on time series of Sentinel-1 radar images allows obtaining satisfactory results given the number of classes (15 classes) and the large number of fields classified. Usually, most studies on crop and land cover classification based on

SAR data consider a limited number of classes, six crop classes (McNairn et al., 2009b; Whelen and Siqueira, 2017), seven land use/land cover classes (Hütt et al., 2016), or less than eleven classes (Bazzi et al., 2019; Larrañaga and Álvarez-Mozos, 2016). Other work has demonstrated the usefulness of Sentinel-1 radar images for mapping cropland and identifying crop phenotype (Arias et al., 2020; Denize et al., 2019; Dingle Robertson et al., 2020; Mestre-Quereda et al., 2020). The SAR multi-temporal polarimetric characteristics, therefore, seem to be a crucial factor to improve crop classification results (Bargiel, 2017), this has been proven by (Larrañaga and Álvarez-Mozos, 2016; Mascolo et al., 2016).

Despite the satisfactory values of PA, UA and F1-score obtained for rice, peanuts, watermelon, water, and uncultivated muddy soil, which can reach 100%, other classes such as forest, uncultivated sandy soil, built-up, and permanent vegetation present less satisfactory results for most scenarios, and the values of PA, UA and F1 score are relatively low, due to confusion with other classes for numerous reasons, such as the forest condition, the built-up area structure, the alternation between crops system, the almost similar backscatter between classes, but mainly time signature confusion.

Permanent vegetation is a class comprising grasses and shrubs located in the vicinity of permanent watercourses, which allows them stability and foliation that are well-developed and rich in water. Thus, these plants record a strong and stable backscatter similar to the time signature of other classes such as avocado trees and built-up classes, which explains the low precision of this class during classification.

The forest area is characterized by an advanced degradation caused by human activities. This permits the development of several herbaceous species with an annual life cycle linked to the presence of rainwater, where they are well developed during winter and spring, and disappear during summer. These companion plants, therefore, record a temporal signature comparable to winter crops, which allowed this class to occupy several parts of the forest area for most of the proposed scenarios. On the other hand, the Laouamra forest is heterogeneous since different species of trees exist with different densities in different parts. The

areas where the density is relatively low allow a stable backscatter compared to citrus, whereas the densest areas give a strong backscatter which can be confused with the permanent vegetation, built-up, or even railway classes for more than one scenario. These confusions are the source of low values of PA, UA, and F1-score.

During the field visits in the summertime, several fields were considered as uncultivated sandy soil; however, the classification results for most of the scenarios give low precision values. This is owing to the assignment of several fields to the classes of winter crops.

The study area is rural and characterized by scattered built-ups in most cases, in addition to villages being restructured during the development of the Loukkos catchment area in the 70's of the last century. This gives a heterogeneity regarding the behavior of these built-ups with the radar waves. Scattered built-ups are most often related to trees and crops around houses, which causes confusion between the built-up and the tree classes. Whereas houses in the restructured villages make it possible to have a backscattering rebound like that of the built ups in the cities, this backscattering is relatively strong and can also lead to confusion with classes of dense trees.

The railway class presents a strong and stable temporal signature linked to the roughness of gravel, which allows the allocation of several strong backscatter classes, such as permanent vegetation and the forest's dense areas to this class, at the time when the pixels attributed to this class are well classified, which explains the high values of PA and the low values of UA.

The bare lands show good results of PA, UA, and F1-score for all the scenarios using the time series, except for the last scenario VH+VV+Texture where the accuracy parameters fall following a strong confusion with the classes of water and winter crops. This could be due to the sensitivity of the textural features, which confused between the low backscatter values of bare land and water, and between the variable backscatter of the annual grasses occupying these lands, and the winter crops.

From these results, we can deduce that there is a link between the backscatter behavior of each class and the attribution of classes in the supervised

classification with the RF classifier algorithm. The classes with distinct temporal profiles and separability are rated the highest, while the classes with an evolution close to other classes and a weak separability give the least satisfactory results. With the phenological evolution, crops of the same type provide similar temporal information on the Sentinel-1 time series image. This allows the classification algorithm to assign the same values to the analyzed crops. Thus, we conclude that the Sentinel-1 time series classification is very effective for monitoring crop and high-resolution mapping, namely for large fields. However, the map resolution decreases when we deal with plants with minor height variation or foliation, which reveals comparable backscatter.

4. Conclusions

This paper aims to explore the potential of Sentinel-1 radar imagery, using time series images in different scenarios to monitor type-crops and land cover mapping in an agricultural area (Laouamra region in the Loukkos Watershed). It is a newly applied approach in Morocco. Obtained results indicate that the Sentinel-1 dual-polarized VV and VH images are suitable for land cover high-resolution mapping using SAR images.

To understand the distribution and to supervise the classification of different classes in the studied area, we undertook a careful analysis of the backscattering behavior evolution from the extracted profiles on the different images covering the study period. This analysis allowed the fine discrimination between crop-types showing consistent backscatter signal with the phenological crop evolution. However, unchanging classes over time display stable backscatter signal through the analyzed period. This analysis was completed by separability and coefficient of variability calculation, and the interpretation of different scenes and RGB color image compositions of the same or different dates. The latter's have been combined with collected data during field visits to assign the pre-processing areas for each class to obtain a high-resolution land cover map of the investigated area.

The use of Sentinel-1 dual-polarized time series SAR imagery has demonstrated a strong potential for multi-temporal analyses required for agricultural fields. Using the RF Classifier algorithm to supervise land cover and crop-types classification we obtain optimal results namely for the crops with height PA, UA, and F1 score parameters, and generally high values of accuracy and the Kappa coefficient (75.19% and 0.73) respectively. This results in a strong discrimination monitoring of fine supervised classification allowing a reliable land cover and crop-types high-resolution mapping for the best-used scenario.

We can therefore confirm the suitability of the multi-temporal monitoring and long-term analysis of crop-types approach used in this work, and generally the use of new technologies such as spatial data for other agricultural fields in Morocco that aims to improve crop-types monitoring and high-resolution mapping techniques, facilitated by the availability of open access sentinel-1 radar images with an exceptional temporal resolution of 6 days.

The new technologies of remote sensing that deals with the classification of confusing classes needs to be enhanced by testing the usefulness of other scenarios in future works through combining polarimetric data with multi-temporal optical data or by using Normalized Difference Vegetation Index (NDVI) optical data.

Supplementary material

Supplementary material is available at https:// polipapers.upv.es/index.php/raet/libraryFiles/ downloadPublic/98

Acknowledgements

References

Abdikan, S., Sanli, F.B., Ustuner, M., Calò, F. 2016. Land cover mapping using Sentinel-1 SAR data. *The International Archives of the Photogrammetry, Remote Sensing and Spatial Information Sciences, Volume XLI-B7, XXIII ISPRS Congress*, 12–19 July 2016, Prague, Czech Republic, 757–761. https://doi. org/10.5194/isprsarchives-XLI-B7-757-2016

Arias, M., Campo-Bescós, M.Á., Álvarez-Mozos, J. 2020. Crop Classification Based on Temporal Signatures of Sentinel-1 Observations over Navarre Province, Spain. *Remote Sensing, 12*, 278. https://doi.org/10.3390/rs12020278

Baghdadi, N., Bernier, M., Gauthier, R., Neeson, I. 2001. Evaluation of C-band SAR data for wetlands mapping. *International Journal of Remote Sensing 22*, 71–88. https://doi.org/10.1080/014311601750038857

Balzter, H., Cole, B., Thiel, C., Schmullius, C. 2015. Mapping CORINE Land Cover from Sentinel-1A SAR and SRTM Digital Elevation Model Data using Random Forests. *Remote Sensing, 7*, 14876–14898. https://doi.org/10.3390/rs71114876

Bargiel, D. 2017. A new method for crop classification combining time series of radar images and crop phenology information. *Remote Sensing of Environment, 198*, 369–383. https://doi.org/10.1016/j.rse.2017.06.022

Bargiel, D., Herrmann, S. 2011. Multi-Temporal Land-Cover Classification of Agricultural Areas in Two European Regions with High Resolution Spotlight TerraSAR-X Data. *Remote Sensing, 3*, 859–877. https://doi.org/10.3390/rs3050859

Bazzi, H., Baghdadi, N., El Hajj, M., Zribi, M., Minh, D.H.T., Ndikumana, E., Courault, D., Belhouchette, H. 2019. Mapping Paddy Rice Using Sentinel-1 SAR Time Series in Camargue, France. *Remote Sensing, 11*, 887. https://doi.org/10.3390/rs11070887

Breiman, L. 1999. *Random Forests-Random Features*. Technical Report, 567, Statistics Department, University of California, Berkeley, 29.

Brisco, B., Ahern, F., Murnaghan, K., White, L., Canisus, F., Lancaster, P. 2017. Seasonal Change in Wetland Coherence as an Aid to Wetland Monitoring. *Remote Sensing, 9*, 158. https://doi.org/10.3390/rs9020158

Brown, S.C.M., Quegan, S., Morrison, K., Bennett, J.C., Cookmartin, G. 2003. High-resolution measurements of scattering in wheat canopies-implications for crop parameter retrieval. *IEEE Transactions on Geoscience and Remote Sensing, 41*(7), 1602–1610. https://doi.org/10.1109/TGRS.2003.814132

Chen, S., Useya, J., Mugiyo, H. 2020. Decision-level fusion of Sentinel-1 SAR and Landsat 8 OLI texture features for crop discrimination and classification: case of Masvingo, Zimbabwe. *Heliyon, 6*, e05358. https://doi.org/10.1016/j.heliyon.2020.e05358

Clauss, K., Ottinger, M., Kuenzer, C. 2018. Mapping rice areas with Sentinel-1 time series and superpixel segmentation. *International Journal of Remote Sensing, 39*, 1399–1420. https://doi.org/10.1080/01431161.2017.1404162

Denize, J., Hubert-Moy, L., Pottier, E. 2019. Polarimetric SAR Time-Series for Identification of Winter Land Use. *Sensors, 19*, 5574. https://doi.org/10.3390/s19245574

Dimov, D., Kuhn, J., Conrad, C. 2016. Assessment of cropping system diversity in the Fergana valley through image fusion of Landsat 8 and Sentinel-1. *ISPRS Annals of Photogrammetry, Remote Sensing & Spatial Information Sciences, 3(7)*, 173–180. https://doi.org/10.5194/isprsannals-III-7-173-2016

Dingle Robertson, L., Davidson, A.M., McNairn, H., Hosseini, M., Mitchell, S., de Abelleyra, D., Verón, S., le Maire, G., Plannells, M., Valero, S., Ahmadian, N., Coffin, A., Bosch, D., Cosh, M.H., Basso, B., Saliendra, N. 2020. C-band synthetic aperture radar (SAR) imagery for the classification of diverse cropping systems. *International Journal of Remote Sensing, 41*, 9628–9649. https://doi.org/10.1080/01431161.2020.1805136

Falcucci, A., Maiorano, L., Boitani, L. 2007. Changes in land-use/land-cover patterns in Italy and their implications for biodiversity conservation. *Landscape Ecology, 22*, 617–631. https://doi.org/10.1007/s10980-006-9056-4

Geymen, A., Baz, I. 2007. Monitoring urban growth and detecting land-cover changes on the Istanbul metropolitan area. *Environmental Monitoring and Assessment, 136*, 449–459. https://doi.org/10.1007/s10661-007-9699-x

Griffiths, P., van der Linden, S., Kuemmerle, T., Hostert, P. 2013. A Pixel-Based Landsat Compositing Algorithm for Large Area Land Cover Mapping. *IEEE Journal of Selected Topics in Applied Earth Observations and Remote Sensing, 6*(5), 2088–2101. https://doi.org/10.1109/JSTARS.2012.2228167

Hansen, M.C., Egorov, A., Roy, D.P., Potapov, P., Ju, J., Turubanova, S., Kommareddy, I., Loveland, T.R. 2011. Continuous fields of land cover for the conterminous United States using Landsat data: first results from the Web-Enabled Landsat Data (WELD) project. *Remote Sensing Letters, 2*, 279–288. https://doi.org/10.1080/01431161.2010.519002

Haralick, R.M., Shanmugam, K., Dinstein, I. 1973. Textural Features for Image Classification. *IEEE Transactions on Systems, Man, and Cybernetics*. SMC-3, 610–621. https://doi.org/10.1109/TSMC.1973.4309314

Harfenmeister, K., Spengler, D., Weltzien, C. 2019. Analyzing Temporal and Spatial Characteristics of Crop Parameters Using Sentinel-1 Backscatter Data. *Remote Sensing, 11*, 1569. https://doi.org/10.3390/rs11131569

Hütt, C., Waldhoff, G. 2018. Multi-data approach for crop classification using multitemporal, dual-polarimetric TerraSAR-X data, and official geodata. *European Journal of Remote Sensing, 51*, 62–74. https://doi.org/10.1080/22797254.2017.1401909

Jeevalakshmi, D., Reddy, S.N., Manikiam, B. 2016. Land cover classification based on NDVI using LANDSAT8 time series: A case study Tirupati region, in: *2016 International Conference on Communication and Signal Processing (ICCSP)*. *IEEE*, Melmaruvathur, Tamilnadu, India, pp. 1332–1335. https://doi.org/10.1109/ICCSP.2016.7754369

Jiancheng S., Dozier, J., Rott, H. 1994. Snow mapping in alpine regions with synthetic aperture radar. *IEEE Transactions on Geoscience and Remote Sensing, 32*, 152–158. https://doi.org/10.1109/36.285197

Khalil, R.Z., Saad-ul-Haque, 2018. InSAR coherence-based land cover classification of Okara, Pakistan. *The Egyptian Journal of Remote Sensing and Space Science, 21*, S23–S28. https://doi.org/10.1016/j.ejrs.2017.08.005

Kpienbaareh, D., Sun, X., Wang, J., Luginaah, I., Bezner Kerr, R., Lupafya, E., Dakishoni, L. 2021. Crop Type and Land Cover Mapping in Northern Malawi Using the Integration of Sentinel-1, Sentinel-2, and PlanetScope Satellite Data. *Remote Sensing, 13*, 700. https://doi.org/10.3390/rs13040700

Kumar, S.D., Rao, S.S., Sharma, J.R. 2013. Radar Vegetation Index as an Alternative to NDVI for Monitoring of Soyabean and Cotton. Indian Cartogr. 33, 91–96.

Kussul, N., Lemoine, G., Gallego, F.J., Skakun, S.V., Lavreniuk, M., Shelestov, A.Yu. 2016. Parcel-Based Crop Classification in Ukraine Using Landsat-8 Data and Sentinel-1A Data. *IEEE Journal of Selected Topics in Applied Earth Observations and Remote Sensing, 9*(6), 2500–2508. https://doi.org/10.1109/JSTARS.2016.2560141

Larrañaga, A., Álvarez-Mozos, J. 2016. On the Added Value of Quad-Pol Data in a Multi-Temporal Crop Classification Framework Based on RADARSAT-2 Imagery. *Remote Sensing, 8*(4), 335. https://doi.org/10.3390/rs8040335

Lee, J.S., Jurkevich, L., Dewaele, P., Wambacq, P., Oosterlinck, A. 1994. Speckle filtering of synthetic aperture radar images: A review. *Remote Sensing Reviews, 8*(4), 313–340. https://doi.org/10.1080/02757259409532206

Mandal, D., Kumar, V., Bhattacharya, A., Rao, Y.S., Siqueira, P., Bera, S. 2018. Sen4Rice: A Processing Chain for Differentiating Early and Late Transplanted Rice Using Time-Series Sentinel-1 SAR Data With Google Earth Engine. *IEEE Geoscience Remote Sensing Letters, 15*(12), 1947–1951. https://doi.org/10.1109/LGRS.2018.2865816

Mandal, D., Kumar, V., Ratha, D., Dey, S., Bhattacharya, A., Lopez-Sanchez, J.M., McNairn, H., Rao, Y.S. 2020. Dual polarimetric radar vegetation index for crop growth monitoring using sentinel-1 SAR data. *Remote Sensing of Environment, 247*, 111954. https://doi.org/10.1016/j.rse.2020.111954

Mascolo, L., López-Sánchez, J.M., Vicente-Guijalba, F., Nunziata, F., Migliaccio, M., Mazzarella, G. 2016. A Complete Procedure for Crop Phenology Estimation With PolSAR Data Based on the Complex Wishart Classifier. *IEEE Transactions on Geoscience and Remote Sensing, 54*(11), 6505–6515. https://doi.org/10.1109/TGRS.2016.2585744

McNairn, H., Champagne, C., Shang, J., Holmstrom, D., Reichert, G. 2009a. Integration of optical and Synthetic Aperture Radar (SAR) imagery for delivering operational annual crop inventories. *ISPRS Journal of Photogrammetry and Remote Sensing, 64*, 434–449. https://doi.org/10.1016/j.isprsjprs.2008.07.006

McNairn, H., Shang, J., Jiao, X. Champagne, C. 2009b. The Contribution of ALOS PALSAR Multipolarization and Polarimetric Data to Crop Classification. *IEEE Transactions on Geoscience and Remote Sensing, 47*(12), 3981–3992. https://doi.org/10.1109/TGRS.2009.2026052

McNairn, H., Shang, J. 2016. A Review of Multitemporal Synthetic Aperture Radar (SAR) for Crop Monitoring, in: Ban, Y. (Ed.), Multitemporal Remote Sensing. Springer International Publishing, Cham, pp. 317–340. https://doi.org/10.1007/978-3-319-47037-5_15

Mestre-Quereda, A., López-Sánchez, J.M., Vicente-Guijalba, F., Jacob, A.W., Engdahl, M.E. 2020. Time-Series of Sentinel-1 Interferometric Coherence and Backscatter for Crop-Type Mapping. IEEE J. Sel. Top. Appl. Earth Observations Remote Sensing, 13, 4070–4084. https://doi.org/10.1109/JSTARS.2020.3008096

Moumni, A., Lahrouni, A. 2021. Machine Learning-Based Classification for Crop-Type Mapping Using the Fusion of High-Resolution Satellite Imagery in a Semiarid Area. *Scientifica, 2021*, 1–20. https://doi.org/10.1155/2021/8810279

Munger, P., Bleiholder, H., Hack, H., Heß, M., Stauss, R., Boom, T., Weber, E. 1998. Phenological Growth Stages of the Peanut Plant (*Arachis hypogaea* L.): Codification and Description according to the BBCH Scale. *Journal of Agronomy and Crop Science, 180*, 101–107. https://doi.org/10.1111/j.1439-037X.1998.tb00377.x

Nasirzadehdizaji, R., Cakir, Z., Balik Sanli, F., Abdikan, S., Pepe, A., Calò, F. 2021. Sentinel-1 interferometric coherence and backscattering analysis for crop monitoring. *Computers and Electronics in Agriculture, 185*, 106118. https://doi.org/10.1016/j.compag.2021.106118

Nasirzadehdizaji, R., Balik Sanli, F., Abdikan, S., Cakir, Z., Sekertekin, A., Ustuner, M., 2019. Sensitivity Analysis of Multi-Temporal Sentinel-1 SAR Parameters to Crop Height and Canopy Coverage. *Applied Sciences, 9*, 655. https://doi.org/10.3390/app9040655

Ndikumana, E., Ho Tong Minh, D., Dang Nguyen, H., Baghdadi, N., Courault, D., Hossard, L., El Moussawi, I. 2018. Estimation of Rice Height and Biomass Using Multitemporal SAR Sentinel-1 for Camargue, Southern France. *Remote Sensing, 10*, 1394. https://doi.org/10.3390/rs10091394

Nelson, A., Setiyono, T., Rala, A., Quicho, E., Raviz, J., Abonete, P., Maunahan, A., Garcia, C., Bhatti, H., Villano, L., Thongbai, P., Holecz, F., Barbieri, M., Collivignarelli, F., Gatti, L., Quilang, E., Mabalay, M., Mabalot, P., Barroga, M., Bacong, A., Detoito, N., Berja, G., Varquez, F., Wahyunto, Kuntjoro, D., Murdiyati, S., Pazhanivelan, S., Kannan, P., Mary, P., Subramanian, E., Rakwatin, P., Intrman, A., Setapayak, T., Lertna, S., Minh, V., Tuan, V., Duong, T., Quyen, N., Van Kham, D., Hin, S., Veasna, T., Yadav, M., Chin, C., Ninh, N. 2014. Towards an Operational SAR-Based Rice Monitoring System in Asia: Examples from 13 Demonstration Sites across Asia in the RIICE Project. *Remote Sensing, 6*, 10773–10812. https://doi.org/10.3390/rs61110773

Panetti, A., Rostan, F., L'Abbate, M., Bruno, C., Bauleo, A., Catalano, T., Cotogni, M., Galvagni, L., Pietropaolo, A., Taini, G., Venditti, P., Huchler, M., Torres, R., Lokas, S., Bibby, D., Geudtner, D. 2014. Copernicus Sentinel-1 Satellite and C-SAR instrument. In: *2014 IEEE Geoscience and Remote Sensing Symposium*. Quebec City, QC, pp. 1461–1464. https://doi.org/10.1109/IGARSS.2014.6946712

Pelletier, C., Valero, S., Inglada, J., Champion, N., Dedieu, G. 2016. Assessing the robustness of Random Forests to map land cover with high resolution satellite image time series over large areas. *Remote Sensing of Environment, 187*, 156–168. https://doi.org/10.1016/j.rse.2016.10.010

Phan, H., Le Toan, T., Bouvet, A. 2021. Understanding Dense Time Series of Sentinel-1 Backscatter from Rice Fields: Case Study in a Province of the Mekong Delta, Vietnam. *Remote Sensing, 13*, 921. https://doi.org/10.3390/rs13050921

Planque, C., Lucas, R., Punalekar, S., Chognard, S., Hurford, C., Owers, C., Horton, C., Guest, P., King, S., Williams, S., Bunting, P. 2021. National Crop Mapping Using Sentinel-1 Time Series: A Knowledge-Based Descriptive Algorithm. *Remote Sensing, 13*, 846. https://doi.org/10.3390/rs13050846

Pulvirenti, L., Squicciarino, G., Cenci, L., Boni, G., Pierdicca, N., Chini, M., Versace, C., Campanella, P. 2018. A surface soil moisture mapping service at national (Italian) scale based on Sentinel-1 data. *Environmental Modelling & Software*, 102, 13–28. https://doi.org/10.1016/j.envsoft.2017.12.022

Selvaraj, S., Haldar, D., Danodia, A. 2019. Time series Sentinel-1A profile analysis for heterogeneous Kharif crops discrimination in North India. *URSI AP-RASC 2019*, New Delhi, India, 09 - 15 March 2019 4 pages.

Song, Y., Wang, J. 2019. Mapping Winter Wheat Planting Area and Monitoring Its Phenology Using Sentinel-1 Backscatter Time Series. *Remote Sensing, 11*, 449. https://doi.org/10.3390/rs11040449

Steinhausen, M.J., Wagner, P.D., Narasimhan, B., Waske, B. 2018. Combining Sentinel-1 and Sentinel-2 data for improved land use and land cover mapping of monsoon regions. *International Journal of Applied Earth Observation and Geoinformation, 73*, 595–604. https://doi.org/10.1016/j.jag.2018.08.011

Suresh, G., Gehrke, R., Wiatr, T., Hovenbitzer, M. 2016. Synthetic Aperture Radar (Sar) Based Classifiers for land applications in Germany. *Int. Arch. Photogramm. Remote Sens. Spatial Inf. Sci.* XLI-B1, 1187–1193. https://doi.org/10.5194/isprsarchives-XLI-B1-1187-2016

Szantoi, Z., Escobedo, F., Abd-Elrahman, A., Smith, S., Pearlstine, L. 2013. Analyzing fine-scale wetland composition using high resolution imagery and texture features. *International Journal of Applied Earth Observation and Geoinformation, 23*, 204–212. https://doi.org/10.1016/j.jag.2013.01.003

Torbick, N., Chowdhury, D., Salas, W., Qi, J. 2017. Monitoring Rice Agriculture across Myanmar Using Time Series Sentinel-1 Assisted by Landsat-8 and PALSAR-2. *Remote Sensing, 9*, 119. https://doi.org/10.3390/rs9020119

Ullman, D.J., LeGrande, A.N., Carlson, A.E., Anslow, F.S., Licciardi, J.M. 2014. Assessing the impact of Laurentide Ice Sheet topography on glacial climate. *Climate of the Past, 10*, 487–507. https://doi.org/10.5194/cp-10-487-2014

Useya, J., Chen, S. 2019. Exploring the Potential of Mapping Cropping Patterns on Smallholder Scale Croplands Using Sentinel-1 SAR Data. *Chinese Geographical Sciences, 29*, 626–639. https://doi.org/10.1007/s11769-019-1060-0

Valcarce-Diñeiro, R., Arias-Pérez, B., Lopez-Sanchez, J.M., Sánchez, N. 2019. Multi-Temporal Dual- and Quad-Polarimetric Synthetic Aperture Radar Data for Crop-Type Mapping. *Remote Sensing, 11*, 1518. https://doi.org/10.3390/rs11131518

Van der Sande, C.J., de Jong, S.M., de Roo, A.P.J. 2003. A segmentation and classification approach of IKONOS-2 imagery for land cover mapping to assist flood risk and flood damage assessment. *International Journal of Applied Earth Observation and Geoinformation, 4*, 217–229. https://doi.org/10.1016/S0303-2434(03)00003-5

Van Tricht, K., Gobin, A., Gilliams, S., Piccard, I. 2018. Synergistic Use of Radar Sentinel-1 and Optical Sentinel-2 Imagery for Crop Mapping: A Case Study for Belgium. *Remote Sensing, 10*, 1642. https://doi.org/10.3390/rs10101642

Vanniel, T., Mcvicar, T., Datt, B. 2005. On the relationship between training sample size and data dimensionality: Monte Carlo analysis of broadband multi-temporal classification. *Remote Sensing of Environment, 98*, 468–480. https://doi.org/10.1016/j.rse.2005.08.011

Veloso, A., Mermoz, S., Bouvet, A., Le Toan, T., Planells, M., Dejoux, J.-F., Ceschia, E. 2017. Understanding the temporal behavior of crops using Sentinel-1 and Sentinel-2-like data for agricultural applications. *Remote Sensing of Environment, 199*, 415–426. https://doi.org/10.1016/j.rse.2017.07.015

Whelen, T., Siqueira, P. 2017. Use of time-series L-band UAVSAR data for the classification of agricultural fields in the San Joaquin Valley. *Remote Sensing of Environment, 193*, 216–224. https://doi.org/10.1016/j.rse.2017.03.014

Whelen, T., Siqueira, P. 2018. Coefficient of variation for use in crop area classification across multiple climates. *International Journal of Applied Earth Observation and Geoinformation, 67*, 114–122. https://doi.org/10.1016/j.jag.2017.12.014

Yan, L., Roy, D.P. 2014. Automated crop field extraction from multi-temporal Web Enabled Landsat Data. *Remote Sensing of Environment, 144*, 42–64. https://doi.org/10.1016/j.rse.2014.01.006

Yunjin, K., van Zyl, J.J. 2009. A Time-Series Approach to Estimate Soil Moisture Using Polarimetric Radar Data. *IEEE Trans. Geosci. Remote Sensing, 47*, 2519–2527. https://doi.org/10.1109/TGRS.2009.2014944

Zakeri, H., Yamazaki, F., Liu, W. 2017. Texture Analysis and Land Cover Classification of Tehran Using Polarimetric Synthetic Aperture Radar Imagery. *Applied Sciences, 7*, 452. https://doi.org/10.3390/app7050452

Zeng, Y., Zhang, J., van Genderen, J.L., Zhang, Y. 2010. Image fusion for land cover change detection. *International Journal of Image and Data Fusion, 1*, 193–215. https://doi.org/10.1080/19479831003802832